PHYSICAL REVIEW B **92**, 125304 (2015)

# Fermi-level pinning through defects at GaAs/oxide interfaces: A density functional study

Davide Colleoni, Giacomo Miceli, and Alfredo Pasquarello
*Chaire Simulation à l'Echelle Atomique (CSEA), Ecole Polytechnique Fédérale de Lausanne (EPFL), CH-1015 Lausanne, Switzerland*
(Received 24 June 2015; published 8 September 2015)

Using density functional calculations, we study a set of candidate defects for Fermi-level pinning at GaAs/oxide interfaces. The set of considered defects comprises both bulklike and interfacial defects, including As antisites, Ga and As dangling bonds, the As-As dimer/dangling bond defect, and several defect complexes. The defects are generated within atomistic model structures representing the $GaAs/Al_2O_3$ interface. Formation energies of bulklike defects are obtained and compared with those of corresponding bulk defects, while interfacial defects are studied through their relative defect energies. Finite-size corrections to the defect energies are applied through a scheme that accounts for the interfacial geometry of our models. Defect levels are defined as thermodynamic transition levels between different charge states and are calculated for all considered defects. Through an alignment procedure based on hybrid functional calculations, the defect levels are then positioned within the calculated band gap of GaAs that reproduces the experimental one, thereby enabling direct comparisons with the experimental density of defect states. Our study shows that several As-related defects show a similar amphoteric bistability between an As-As dimer state and a configuration with two doubly occupied As dangling bonds. The associated charge transition levels generally lie in the midgap region, in accord with experimental observations. This mechanism is proposed as the origin of the observed Fermi-level pinning at GaAs/oxide interfaces.

DOI: 10.1103/PhysRevB.92.125304 PACS number(s): 31.15.A−, 73.20.Hb

## I. INTRODUCTION

Among the class of III-V compounds, GaAs is the prototype material presently considered as a replacement for silicon in complementary-metal-oxide-semiconductor (CMOS) technology owing to its high electron mobility [1,2]. However, the development of a GaAs-based technology is held back by the low quality of GaAs/oxide interfaces [3,4]. Indeed, a high density of interfacial defect states is found to prevent the proper operation of GaAs-based devices through Fermi-level pinning [4,5].

For GaAs, Fermi-level pinning is observed at the interface with typical oxides [3–6], at the surface upon submonolayer deposition of various metals or oxygen [7–10], and in the bulk either upon oxygen doping [11–15] or high-energy irradiation [16–18]. The occurrence of defects has been suggested to underlie all these observations. Nevertheless, the energy at which the Fermi level is pinned depends on the specific GaAs-based system, thus suggesting that different pinning mechanisms are operative.

Fermi-level pinning due to defects could be understood assuming that the defects give rise to a high density of defect states within the semiconductor band gap. However, a different mechanism based on the occurrence of amphoteric defects has been proposed by Walukiewicz [16]. Such defects could be formed either as acceptors or as donors depending on the position of the Fermi energy in the band gap. In turn, the formation of such amphoteric defects then affects the position of the Fermi level, pushing it towards higher energy when a donor defect is created or towards lower energy when an acceptor defect is created. This feedback mechanism leads to the pinning of the Fermi level at the energy where the donor and the acceptor character of the defect coexist.

Focusing on GaAs/oxide interfaces, a high concentration of interfacial defects is generated when the oxides are grown on GaAs substrates through atomic layer deposition [19–28]. The measured density of interface states ($D_{it}$) shows minor peaks in the vicinity of both the valence and the conduction band. These peaks have been shown to be responsive to sulfur passivation [4,5,29]. However, the major peak located at midgap (∼0.7 eV above the valence band maximum) has eluded passivation and has thus been identified as the major obstacle for using GaAs in CMOS devices [4,5,26]. Density-of-states measurements indicate that the midgap peak separates donorlike from acceptorlike defect states, thereby favoring the mechanism based on amphoteric defects as origin of Fermi-level pinning in GaAs [6]. Experimental observations, such as the As interfacial enrichment upon oxidation [30] and the reduction of the midgap defect density when using Ga-rich surfaces prior to oxidation [5], suggest that the defect responsible for this peak is related to arsenic. The experimental characterization is further complicated by the realization of unpinned GaAs/oxide interfaces obtained through molecular beam epitaxy (MBE) [3,31–33].

Significant insight into the role of specific defects has recently been acquired through the use of density functional calculations [34–45]. The small peaks in the density of defect states close to the valence and conduction band edges have thus been assigned to As and Ga dangling bonds (DBs) [36,42]. The antibonding state of the As-As dimer has also been proposed to give defect states close to the conduction-band minimum (CBM) [38,40,42,44]. As far as the midgap peak is concerned, there are both experimental and theoretical indications that point to the As antisite defect [30,46,47], but a detailed identification based on precise peaks in the measured $D_{it}$ is still lacking [43]. More recently, it has been suggested that the As-As dimer/DB defect acts as the dominant defect at GaAs/oxide interfaces [43,45]. The As-As dimer/DB defect shows a bistability between an As-As dimer and two doubly occupied dangling bonds ($2\,DB^{\bullet}_{As}$). Its amphoteric nature provides a mechanism for Fermi-level pinning and its donor/acceptor character agrees with the experimental characterization of the midgap peak in the $D_{it}$ [6].

Several GaAs-based systems other than GaAs/oxide interfaces also show Fermi-level pinning due to defects. Upon

 

a high dose of irradiation, the Fermi energy in bulk GaAs is found to stabilize at ∼0.6 eV from the valence band maximum (VBM), regardless of its initial position in the band gap [16–18]. This behavior has initially been assigned to the amphoteric nature of bistable Ga vacancies [48]. More recently, a defect complex involving an As vacancy ($V_{As}$) and two As antisites ($As_{Ga}$) has been proposed [49]. This defect also occurs in the form of a $V_{Ga}$-$As_{Ga}$ complex, and is here denoted as $V_{Ga}$-$As_{Ga}$/$V_{As}$-2 $As_{Ga}$. This complex is not only amphoteric like the Ga vacancy but is also predicted to have a defect level in correspondence of the pinned Fermi level. In oxygen-doped GaAs, Fermi-level pinning occurs at ∼1.1 eV above the VBM [11,15], presumably due to oxygen-related defects. The rich experimental characterization [11–15,50–53] combined with density functional studies [54,55] have enabled the identification of the $(As_{Ga})_2$-$O_{As}$ defect consisting of a Ga-O-Ga unit next to two As antisites. In particular, recent hybrid-functional calculations for this defect have yielded excellent quantitative agreement with experiment for both the position of the pinned Fermi level and the optical transitions between its different charge states [55]. Defect-induced Fermi-level pinning has also been observed at GaAs surfaces. The deposition of only a small amount of various metals or oxygen is sufficient to pin the Fermi level [7–10]. The pinning occurs in correspondence of the energy levels of $As_{Ga}$ defects offering a straightforward assignment [7]. However, more recently, an alternative interpretation based on the formation of the As-As dimer/DB defect has been suggested [43].

In this work, we present an extensive density functional study of GaAs defects in view of identifying likely candidates for Fermi-level pinning at GaAs/oxide interfaces. We model the defects in the vicinity of the interface adopting atomistic models of the GaAs/$Al_2O_3$ interface as parent structures. The set of considered defects includes typical bulk defects, such as the As antisite [30,56], the $V_{Ga}$-$As_{Ga}$/$V_{As}$-2 $As_{Ga}$ defect complex [49], and the $(As_{Ga})_2$-$O_{As}$ defect [54,55], but also interfacial defects, such as the Ga dangling bond [36,42], the As dangling bond [36], and the As-As dimer/DB defect [38,40,42,43]. All these defects have been related to the occurrence of Fermi-level pinning, and are here treated on an equal footing using the same computational setup. Our assignment scheme is based on the accurate determination of defect levels and on the comparison with the experimental $D_{it}$, in particular with the goal of identifying the origin of its midgap peak. Therefore, special attention is paid in our study to align the calculated levels with respect to the GaAs band edges through the use of hybrid functional calculations and to the treatment of finite-size effects resulting from the use of an interface geometry. In particular, in the case of bulk defects, the effect of the near-interface location is addressed in comparison to a location in the bulk.

The paper is organized as follows. In Sec. II, we describe our theoretical approach. In particular, this section contains a description of the interfacial models used, an outline of our scheme for the calculation and the alignment of defect levels, and a discussion illustrating the distinction between bulklike defects and interfacial defects. The results of our calculations for bulklike defects and interfacial defects are given in Secs. III and IV, respectively. In Sec. V, a direct comparison between our results and the experimental density of interface states is presented and conclusions are drawn.

## II. METHODS

### A. Electronic-structure method

All the defect models in this work have undergone full structural relaxation within a density-functional-theory (DFT) scheme in which the electronic structure is described through the semilocal functional proposed by Perdew, Burke, and Ernzerhof (PBE) [57]. We use plane-wave basis sets together with norm-conserving pseudopotentials, as provided in the QUANTUM-ESPRESSO suite of programs [58]. The basis sets are defined by a kinetic energy cutoff of 70 Ry. For the bulk calculations of the bulklike defects, we used a 64-atom supercell and an off-center translated $2 \times 2 \times 2$ **k**-point mesh, which has been found to yield converged results [59]. In the interface calculations, the supercell size is twice as large in the direction perpendicular to the interface. We thus sample the Brillouin zone of the supercell through a $2 \times 2 \times 1$ **k**-point mesh which results in the same **k**-point density as in the bulk calculations.[1]

For determining the band edges of GaAs, we perform hybrid functional calculations for bulk GaAs. We use the hybrid functional proposed by Heyd, Scuseria, and Ernzerhof (HSE) [60,61], as implemented in the QUANTUM-ESPRESSO code [62,63]. The range-separation parameter is kept fixed at its original value ($\mu = 0.11$ bohr$^{-1}$ [61]) to preserve the overall accuracy of the functional [62]. At variance, the fraction of nonlocal Fock exchange is set to $\alpha = 0.35$ to reproduce the experimental band gap GaAs ($E_g = 1.52$ eV [64]) following the scheme outlined in Ref. [56]. This results in conduction-band and valence-band shifts of +0.42 and −0.47 eV with respect to the PBE band edges, respectively. We then position the defect charge transition levels calculated at the PBE level within this enlarged band gap by aligning the average electrostatic potential in the PBE and HSE calculations [65–67]. Indeed, for well-localized defect states, defect levels calculated at the semilocal and at the hybrid-functional level have been shown to agree closely provided such an alignment scheme is adopted [62,68,69]. This general feature allows one to use a computationally inexpensive functional such as PBE, while retaining the same accuracy as achieved with the full HSE calculation [43,66]. Focusing on the As-As dimer/DB defect, we showed that the defect level obtained with our alignment scheme and the corresponding one obtained with the HSE functional differ by only ∼0.02 eV [67]. This incertitude is negligible as it is considerably smaller than typical errors affecting defect calculations. Through a benchmark study on the As antisite in GaAs, the latter have been estimated to be about 0.2 eV [56].

The application of the alignment scheme described above relies on a sufficiently large band gap at the PBE level. In our interface calculations, this condition is achieved as a consequence of the quantum-confinement effect associated

[1]In this case, it was unnecessary to resort to an off-center **k**-point mesh as the gap is opened through the quantum confinement effect.

to the GaAs slab calculation. Similarly, in our bulk PBE calculations, a large band gap is achieved through the use of an off-center **k**-point mesh.

The structural relaxations in the approach used in this work are carried out at the semilocal level and do not account for particular relaxation effects that might occur at the hybrid functional level. However, insofar as the hybrid functional preserves the bonding properties achieved at the semilocal level, such relaxations generally lead to minimal changes, both as far as the structure and the charge transition levels are concerned. For example, a full HSE calculation for the As antisite in GaAs gives charge transition levels at 0.51 and 0.92 eV above the VBM [56], to be compared with the values of 0.53 and 0.96 eV found in this work through our PBE-based approach (see below). In particular circumstances, due to an improved description of the self-interaction, structural optimization at the hybrid functional level may lead to asymmetric relaxations favoring the localization of the defect wave function [70–73]. In such cases, the defect state results from a competition between a symmetric and an asymmetric state, which generally does not affect the charge transition levels in a significant way [72].

### B. Parent interface models

The defect structures are created within two parent model structures of the $GaAs/Al_2O_3$ interface (see Fig. 1). Both models originate from previously generated structures [40,47]. The original models have undergone full structural relaxation upon minor modifications ensuring that the semiconductor-oxide interface is characterized by Ga-O bonds, as suggested from the interpretation of As $2p$ core-level spectra [47].

Model I consists of 227 atoms in a tetrahedral supercell and is shown in Fig. 1(a). The repeat interface unit in the direction parallel to the interface contains eight interface atoms of GaAs. The oxide slab is modeled by the $\kappa$ phase of crystalline $Al_2O_3$, which shows a mass density and atomic coordinations similar to those of amorphous alumina grown through atomic layer deposition [74]. The interface pattern is obtained by superimposing $\kappa$-$Al_2O_3$(011) to GaAs(001) and allowing for small lateral strains. For GaAs, we use the experimental lattice parameter of 5.65 Å [64], which corresponds to a bulk bond length of 2.45 Å.

Model II has been designed to model the As-As dimer/DB defect [40]. Model II is obtained from model I by displacing the oxide slab and the interfacial Ga layer along the [110] direction until the Ga atoms lie atop of the As atoms. Upon structural relaxation, the interfacial Ga and As atoms then form an equal number of As-As and Ga-Ga dimers. Oxygen atoms are subsequently inserted in the dimer bonds until a single As-As dimer remains, as shown in Fig. 1(b).

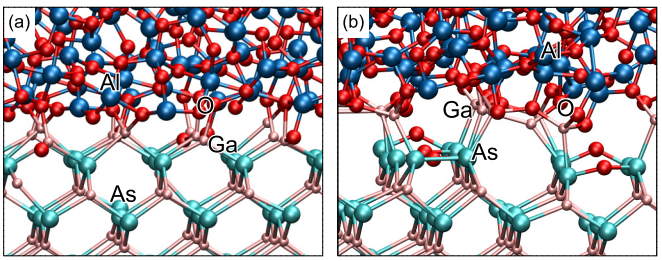


FIG. 1. (Color online) Atomic structures of two parent $GaAs/Al_2O_3$ interface models considered in this study: (a) model I and (b) model II. Model II contains an interfacial As-As dimer which is shown in the foreground in (b).

It is important to remark that the structures in both model I and model II satisfy electron-counting-rule arguments, which are expected to govern the local electronic structure in III-V semiconductors [38,75]. In the bulk, Ga and As atoms are tetrahedrally coordinated contributing to each bond with 3/4 and 5/4 electrons, respectively. This ensures that all bonds carry two electrons as required for closed shell systems. In interface model I, a substrate layer of As atoms bonds continuously to an oxide layer of cations, which are trivalent and thereby satisfy the electron counting rule. As far as interface model II is concerned, the electron counting rule is also satisfied as the excess 1/2 electrons released by the formation of an As-As bond are required to saturate the formation of a Ga-Ga bond. We note that the addition of an O atom in a homopolar bond does not modify the electron counting, as a twofold-coordinated O atom contributes with one electron per bond.

### C. Defect formation energies and defect levels

In this study, the defect levels correspond to thermodynamic charge transition levels and are obtained through the defect formation energies of different charge states as a function of Fermi energy. The charge transition levels then correspond to Fermi energies at which the formation energies of the involved charge states are equal.

For an isolated defect $X$ at the interface, we calculate its formation energy $E_f[X^q]$ in its charge state $q$ as a function of the Fermi energy $\epsilon_F$ given with respect to the valence band maximum ($\epsilon_v$) [76]:

$$E_f[X^q] = E_{tot}[X^q] + E^q_{corr} - E_{tot}[\mathrm{ref}] - \sum_i n_i\mu_i + q[\epsilon_F + \epsilon_v + \Delta v_{0/b}], \quad (1)$$

where $E_{tot}[X^q]$ is the total energy of the supercell with the defect $X$ in charge state $q$ and $E_{tot}[\mathrm{ref}]$ the total energy of the defect-free reference supercell. For each species $i$, the chemical potential $\mu_i$ of the $n_i$ added (or removed) atoms allows us to describe various growth conditions. In this work, we consider the As-rich condition in which $\mu_{As}$ corresponds to the tetrahedral $As_4$ molecule, and $\mu_{Ga}$ is derived from the equilibrium condition with GaAs, $\mu_{Ga} = \mu_{GaAs} - \mu_{As}$. $\mu_O$ is taken to correspond to the isolated $O_2$ molecule. $\epsilon_v$ is the VBM of bulk GaAs as obtained from a separate bulk calculation. $\Delta v_{0/b}$ is a potential alignment term which accounts for the potential shift between the calculations of bulk GaAs and of the neutral interfacial defect [76,77].

In this work, we apply a finite-size correction $E^q_{corr}$ that accounts for the long-range nature of the Coulomb interaction and the use of periodic boundary conditions. The applied corrections are in the spirit of the method proposed by Freysoldt, Neugebauer, and Van de Walle [78] but generalized to the superlattice geometry used for modeling the interface [79]. The defect charge is modeled through a Gaussian distribution with

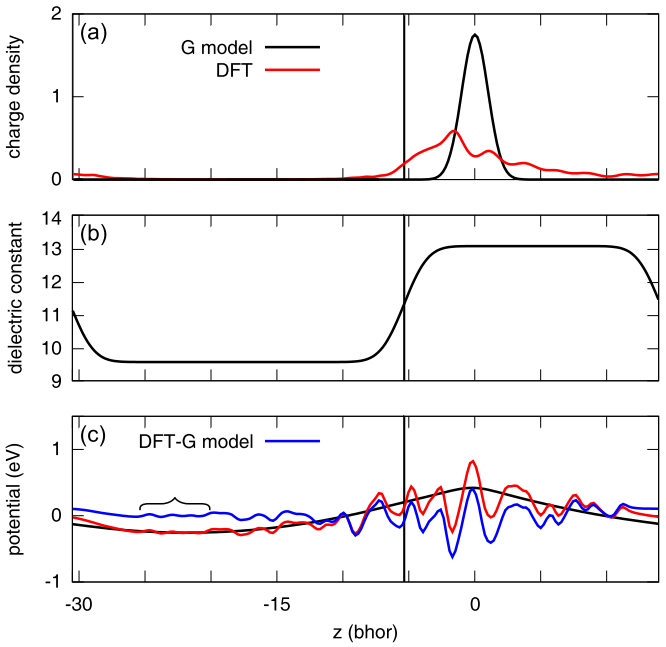


FIG. 2. (Color online) (a) Planar-averaged distributions of the Gaussian model charge (G model, black line) and of the $As_{Ga}$ defect charge in the +2 charge state as found in a DFT calculation at the PBE level (red line). The defect is located at the origin and the interface is visualized through a vertical line. (b) Dielectric constant profile across the interface as used in the present work. (c) Planar averages of the DFT-PBE electrostatic potential obtained as difference between the potentials of the +2 charged and the neutral $As_{Ga}$ defect. The blue line represents the short-ranged defect potential and is obtained as the difference between the red and the black lines. The accolade indicates a region far from the defect in which the short-ranged potential is found to be constant.

a width of 1 bohr [Fig. 2(a)] and the dielectric-constant profile is described through an error function with a smoothness parameter of 2 bohr [Fig. 2(b)]. For the bulk dielectric constants of GaAs and $Al_2O_3$, we use experimental values of 13.1 [80] and 9.6 [81], respectively. The size of largest finite-size corrections obtained in this work are of the order of 0.2–0.4 eV for defects in the charge states ±2. The detailed parameters defining the dielectric-constant profile are not critical. For instance, using theoretical dielectric constants or any other smoothness parameter ranging between 0.5 bohr and 4 bohr affects the corrections by less than 20 meV. The electrostatic potential generated by the Gaussian charge reproduces well the DFT potential obtained from the difference between the defect potentials in the charged and neutral charge states [Fig. 2(c)]. The resulting short-range potential is obtained from the difference of the DFT and the model potential and shows a flat behavior far from the defect, thereby ensuring that the defect charge distribution is well localized [75].

### D. Bulklike defects and interfacial defects

In this work, we consider two types of defects located in the vicinity of the interface. The first type of defects have corresponding isolated defects in the bulk and their sole difference is their proximity to the interface. We refer to these defects as bulklike defects. This set includes the $As_{Ga}$ defect, the $(As_{Ga})_2$-$O_{As}$ defect, and the $V_{As}$-2 $As_{Ga}$ defect complex. These defects are here modeled at interface model I. In this case the defect-free interface can be taken as reference in order to define the defect formation energy as described in Eq. (1).

Next, we also consider another type of defects that does not have corresponding bulk defects. These defects are peculiar to GaAs terminations such as surfaces or interfaces. We refer to this type of defects as to interfacial defects. Defects considered here and belonging to this type are the Ga DB, the As DB, and the As-As dimer/DB defect. Such defects generally require specific models such as interface model II. When such defects are created within periodic defect-free structures, the periodicity is interrupted and can be restored only through the introduction of secondary defective structural units. The absence of a defect-free reference system which differs from the defect only by the appearance of the defect itself prevents the definition of absolute formation energies. For these defects, only relative formation energies of different charge states can be calculated.

The secondary structural units formed upon the creation of such defects in previously defect-free systems may not satisfy locally the electron counting rule and thus carry a charge $q'$. For instance, in interface model II, the formation of the As-As dimer occurs in combination with the formation of the interfacial Ga-O-Ga and As-O-As structures. When the local charges are defined through electron counting arguments, the As-As dimer is in a charge state $q = 0.5$, while the Ga-O-Ga and As-O-As structures globally carry a compensating charge of $q' = -0.5$. From this reasoning it follows that the charge of the supercell $Q$ does not necessarily correspond to the charge $q$ carried by the defect of interest. Indeed, the total supercell charge $Q$ corresponds to the sum of all local charges in the supercell, namely the sum of the defect charge $q$ and of the charge $q'$ of the secondary structural units. Moreover, in order to study the energy levels of the defect of interest, it is a necessary condition that upon charging the secondary structural units remain electrically inactive, i.e., that their charge $q'$ does not vary. For this reason, we inserted O atoms into all homopolar bonds but one in the generation of interface model II.

For the electronic properties of interfacial defects, we follow a two-step procedure [43]. First, we obtain the defect energy $\Delta E^Q$ corresponding to the supercell with charge $Q$:

$$\Delta E^Q = E^Q_{\rm tot} + E^Q_{\rm corr} - E_{\rm ref} + Q\epsilon_{\rm F}, \qquad (2)$$

where $E^Q_{\rm tot}$ is the total energy of the supercell and $E^Q_{\rm corr}$ the finite-size correction as it appears in Eq. (1). As discussed, only the relative defect energies are accessible and a constant reference energy $E_{\rm ref}$ remains undefined. For simplicity, we fix $E_{\rm ref}$ such that the defect energy $\Delta E^Q$ vanishes for $\epsilon_{\rm F} = \epsilon_{\rm v}$. Any secondary structural units do not undergo any charge transition for Fermi energies within the band gap. Thus, their energy as function of $\epsilon_{\rm F}$ shows a linear dependence with a slope defined by their charge $q'$. To the extent that $q$-$q'$ interactions are negligible, it is then possible to obtain the defect energy $\Delta E^q$ pertaining to the sole defect of interest through the following subtraction [43]:

$$\Delta E^q = \Delta E^Q - q'\epsilon_{\rm F}. \qquad (3)$$

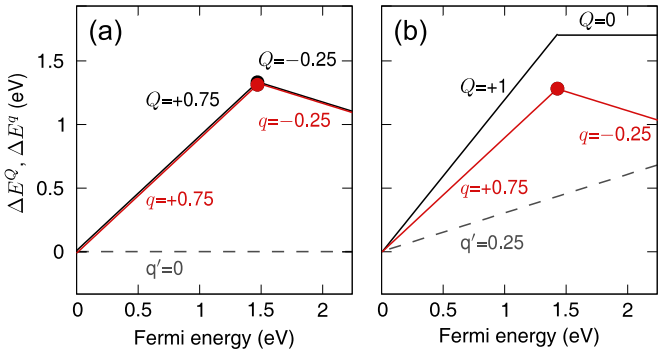


FIG. 3. (Color online) Defect energy of an interfacial Al DB defect in bulk AlAs with different secondary structural units: (a) pseudo-H atoms saturate the As DBs in the cavity leading to neutral secondary structural units ($q' = 0$), (b) one of the pseudo-H is replaced by a regular hydrogen atom leading to $q' = 0.25$.

The relative defect energies obtained in this way are sufficient for determining the defect charge transition levels. However, in absence of absolute formation energies, it is not possible to establish any link with the defect abundances at thermodynamic equilibrium.

In order to illustrate the calculation of charge transition levels through this procedure, we consider an Al DB defect in a 64-atom bulk supercell of AlAs at the PBE level.[2] We focus on AlAs rather than on GaAs because the large band gap of AlAs encloses the DB defect levels already at the PBE level [36], while AlAs is equivalent to GaAs from the electron counting point of view. To generate the Al DB model, a cavity is created in the bulk structure by removing four atoms (one As and three Al atoms). All the undesired As DBs are then saturated with pseudo-H atoms carrying 3/4 electrons [82]. In this model, the pseudo-H represent the secondary structural units that are required to restore the bulk periodicity. These structures locally satisfy the electron counting rule leading to $q' = 0$ and $Q = q$. We consider the charge transition between the empty and the singly occupied DB, corresponding to charged calculations in which $Q = q = +0.75$ and $Q = q = -0.25$, respectively. In this case, the defect energies $\Delta E^Q$ and $\Delta E^q$ coincide, as shown in Fig. 3(a), where the energy scale is referenced with respect to the defect energy at the VBM. The charge transition level is found at 1.48 eV above the VBM.

To examine the possible role of $q$-$q'$ interactions, it is interesting to note that the charge transition level calculated above closely agrees with the result of 1.37 eV obtained in Ref. [36] with different secondary structural units, namely a six-atom cavity (three As and three Al atoms) and a saturation with regular H atoms. To further explore such effects, we replace one pseudo-$^{0.75}$H with a regular H atom and repeat the calculations for the Al DB. Since the H-As bond releases 1/4 electrons to locally fulfill the electron counting rule, this modification leads to charged secondary units with $q' = +0.25$. Hence, the singly occupied DB ($q = +0.25$) in this setup corresponds to a neutral supercell with $Q = 0$, while the empty DB is achieved with a supercell charge of $Q = +1$. The corresponding defect energies $\Delta E^Q$ and $\Delta E^q$ are shown in Fig. 3(b). By comparing the two panels in Fig. 3, one notices that $\Delta E^Q$ substantially depends on the choice of secondary units, while $\Delta E^q$ barely changes and thus reliably reflects the properties of the defect of interest. Indeed, the charge transition level calculated within the two approaches differs by only 0.06 eV. This difference might be taken as an estimate of the effect of the neglected $q$-$q'$ interactions in this case.

Estimating the size of the $q$-$q'$ interactions in general might not be trivial and is expected to depend on the size of the charge $q'$ and on its location with respect to the defect charge $q$. In Ref. [43], an extreme case has been considered corresponding to the addition of a $Mg^{2+}$ ion among the secondary structural units. Nonetheless, the charge transition level of the defect under investigation was found to shift by less than 0.2 eV. Such an error still does not exceed typical incertitudes associated to density functional calculations [56].

## III. BULKLIKE DEFECTS

### A. $As_{Ga}$ defect

We model the $As_{Ga}$ in the first Ga layer on the GaAs side of interface model I, as shown in Fig. 4(a) for the neutral defect charge state. In the bulk, the $As_{Ga}$ defect is stable in the neutral, the singly positive, and the doubly positive charge states [56]. The neutral charge state exhibits a metastability, which has been associated to the EL2 defect [83,84]. The metastable configuration ($As^{\star}_{Ga}$) shows the As antisite atom occupying a $C_{3v}$ position upon the breaking of one As-As bond and the relaxation to a nearby interstitial site. Application of the electron counting rule [38,75] reveals that the neutral $As_{Ga}$ possesses two electrons in excess. In the stable neutral charge state, the two electrons are delocalized over the antisite atom and its As-As bonds, while they are localized in two doubly occupied As DBs in the metastable configuration.

Here, we consider the three stable charge states and the neutral metastable state for a location of the antisite in

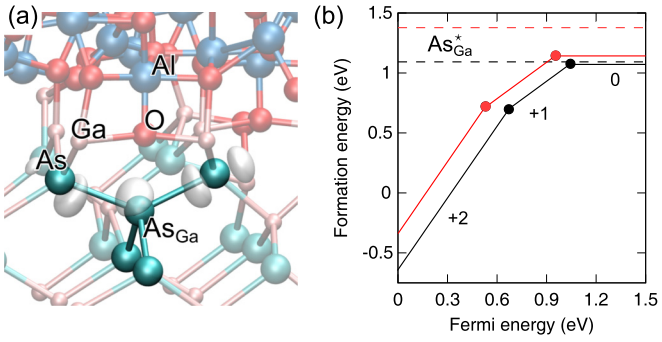


FIG. 4. (Color online) (a) Relaxed structure of the $As_{Ga}$ defect in the stable neutral charge state. The charge density of the defect state is shown in transparency. (b) Formation energy vs Fermi energy for the $As_{Ga}$ defect as obtained through the use of model I of the $GaAs/Al_2O_3$ interface (black lines) and of a bulk model (red lines). The dashed lines correspond to the energy of the corresponding $As^{\star}_{Ga}$ defects. As-rich conditions are assumed.

[2]The Brillouin is sampled at the Γ point; other computational parameters follow Ref. [36]. For the finite-size corrections we use the experimental value of the dielectric constant ($\epsilon = 10.06$ [80]).

proximity of the interface. In the most stable neutral state, there is a small departure from the tetrahedral symmetry. The bond length of the As-As bonds pointing to the $Al_2O_3$ component of the interface are ∼2.59 Å, 0.07 Å longer than those pointing to the GaAs component of the interface (∼2.52 Å). From the inspection of the defect charge density given in Fig. 4(a), we note that the structural asymmetry is associated with a preferential electron localization on the As atoms located closer to the interface. This can be understood by the attraction exerted by the highly polar Ga-O bonds at the interface. In the positive charge states, the As-As bond lengths become shorter and the overall structure of the defect core shows smaller deviations from tetrahedral symmetry. In particular, in the +2 charge state, the As-As bond lengths are ∼2.47 Å on the GaAs side and ∼2.48 Å on the oxide side.

The $As^{\star}_{Ga}$ configuration at the interface can be generated by breaking an As-As bond either on the semiconductor side of the antisite or on the oxide side of the antisite. In both cases the $As^{\star}_{Ga}$ configuration is higher in energy than the near-tetrahedral $As_{Ga}$. When the bond breaking occurs on the semiconductor side the metastable $As^{\star}_{Ga}$ is higher in energy by only 0.02 eV, whereas the bond breaking on the oxide side yields a metastable $As^{\star}_{Ga}$ at 0.23 eV, not far from the value of 0.24 eV found for a location in the bulk. This indicates that the $As^{\star}_{Ga}$ configuration with a bond breaking on the semiconductor side is stabilized at the interface. This effect can be assigned to the more significant backward relaxation of the antisite atom for displacement towards the oxide. In its most stable configuration, the $As^{\star}_{Ga}$ defect shows an average As-As bond length of 2.48 Å while the distance between the two As atoms carrying a doubly occupied DB is 3.52 Å.

The formation energies vs Fermi energy for the stable charge states of the $As_{Ga}$ defect are given in Fig. 4(b). The antisite defect shows a double-donor behavior, in which the neutral, the singly positive, and the doubly positive charge states are the most stable ones. The $\varepsilon_{+2/+1}$ and $\varepsilon_{+1/0}$ charge transition levels lie at 0.67 eV and 1.04 eV above the GaAs VBM. In this calculation, the finite-size corrections applied to the defect formation energies amount to 0.10 eV and 0.40 eV for the +1 and +2 charge states, respectively. For comparison, Fig. 4(b) also shows our calculated formation energies for the $As_{Ga}$ in the bulk, which yield defect levels at 0.51 and 0.91 eV above the VBM. Our bulk results agree well with previous results in the literature [59,62], from which they differ only by the use of a different finite-size correction scheme. The comparison shows that the defect levels of the $As_{Ga}$ shift by only 0.15 eV to higher energies when the defect is located close to the interface, suggesting that the electrical properties remain similar. However, the defect formation energies in the positive charge states are lower. In particular, for *p*-type conditions, the formation energy decreases by ∼0.45 eV, suggesting that the defect incorporation is facilitated at the interface.

Recent electron spin resonance experiments have provided support for the occurrence of $As_{Ga}$ antisite defects at GaAs/oxide interfaces [30]. Furthermore, specific features in the As 2*p* core-level spectra [22] can be assigned to the $As_{Ga}$ antisite [47]. Therefore, this defect has often been proposed for being responsible of the midgap peak in the experimental density of interface states [30,46,47]. Density-of-states measurements have reported the occurrence of two midgap peaks, one of donorlike states at 0.5 eV and one of acceptorlike states at 0.9 eV above the VBM [4,6]. Other measurements on interfaces grown in As-rich conditions report the presence of a single midgap peak at 0.7 eV above the VBM [5]. Such density-of-states experiments are subject to incertitudes of 0.2 eV due to estimates of defect cross sections [4], and thus prevent any conclusive statement concerning the number of peaks. Nevertheless, most of these observations are compatible with the $As_{Ga}$ defect. This defect introduces defect levels in the midgap region of the GaAs band gap and is consistent with the As enrichment observed at the interface [22,23,30,85,86]. However, it acts as a double donor and therefore it completely lacks the acceptorlike behavior observed experimentally [6]. Moreover, because of its donor properties, the occurrence of sole As antisite defects cannot stabilize the Fermi level without the participation of an acceptorlike defect [87]. Thus, despite clear experimental evidence supporting the occurrence of $As_{Ga}$ antisites at the GaAs/oxide interfaces [30], these defects cannot trivially account for the observed Fermi-level pinning.

### B. $(As_{Ga})_2$-$O_{As}$ defect

The $(As_{Ga})_2$-$O_{As}$ defect is composed of two As antisite defects, which are nearest neighbors in the Ga sublattice and separated by an As vacancy, in which an O atom is captured. The relaxed structure at the interface is shown in Fig. 5(a). In bulk GaAs, this defect is stable in the singly positive and singly negative charge states, while it is metastable in the neutral charge state. The amphoteric behavior of this defect accounts for the Fermi-level pinning in oxygen-doped GaAs [55], with the calculated +1/−1 charge transition level in excellent agreement with the measured position of the pinned Fermi energy [11,15].

In proximity of the interface, this defect shows many similarities with its bulk counterpart. The stable charge states are still the +1 and −1 charge states, both satisfying the electron counting rule. In the +1 charge state, each of the two As antisite atoms forms three As-As bonds and one As DB leading to an overall release of 3/2 electrons, of which 1/2 electron account for the saturation of the Ga-O-Ga unit. The As-As bond lengths are 2.49 ± 0.01 Å and the

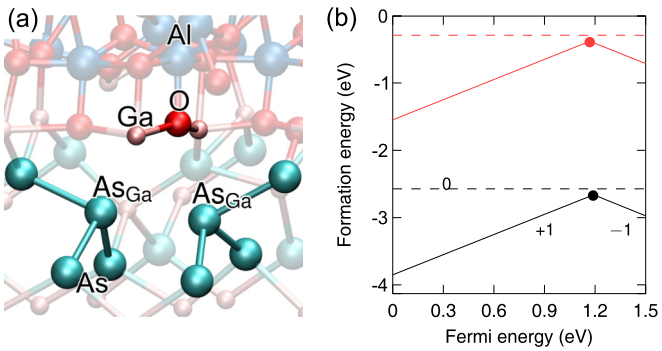


FIG. 5. (Color online) (a) Relaxed structure of the $(As_{Ga})_2$-$O_{As}$ defect in the metastable neutral charge state. (b) Formation energy of the $(As_{Ga})_2$-$O_{As}$ defect vs Fermi energy as obtained through the use of model I of the GaAs/$Al_2O_3$ interface (black lines) and of a bulk model (red lines). The bulk result is taken from Ref. [55]. As-rich conditions are assumed.

distance between the As antisite atoms is 3.61 Å. The O atom is threefold coordinated forming two Ga-O bonds of ∼1.9 Å and one Al-O bond of 1.82 Å. Upon electron capture, the defect structure undergoes structural rearrangements that mostly involve the As atoms of the defect core, in analogy to the defect behavior in the bulk [55]. In the −1 charge state, the two antisite atoms move closer and form a bond, while each of them breaks one of its As-As back bonds giving four doubly occupied DBs in total. In this configuration, the average As-As bond length is 2.52 Å and the $As_{Ga}$-$As_{Ga}$ bond length is 2.70 Å, while the structural unit involving the O atom undergoes minimal variations. In the neutral charge state, the defect structure is similar to that of −1 defect state, with the $As_{Ga}$-$As_{Ga}$ bond being only singly occupied.

The transformation of the defect structure from the +1 to the −1 charge state only involves the defect As atoms, leaving the Al–O–$Ga_2$ unit unchanged. The capture of two electrons can thus be expressed as:

$$2\,DB^{\bullet}_{As} + 2\,\text{As-As} \underset{-2e^-}{\overset{+2e^-}{\rightleftharpoons}} 4\,DB^{\bullet}_{As} + \text{As-As}, \tag{4}$$

which can be simplified to give:

$$\text{As-As} \underset{-2e^-}{\overset{+2e^-}{\rightleftharpoons}} 2\,DB^{\bullet}_{As}. \tag{5}$$

This reaction thus corresponds to an As-As dimer breaking up into two opposite doubly occupied As DBs, a transformation which has recently been identified to be common to various GaAs systems [43].

The formation energies of the $(As_{Ga})_2$-$O_{As}$ defect are shown as a function of the Fermi energy in Fig. 5(b). Calculated finite-size correction energies are about 0.1 eV for both the positive and the negative charge state. The amphoteric behavior of the defect could lead to Fermi-level pinning at the +1/−1 charge transition, found at 1.19 eV above the GaAs VBM. Compared to the same defect in the bulk [cf. Fig. 5(b)] [55], the defect level shifts by only 0.05 eV towards higher energy. However, the formation energy drops by more than ∼2 eV, suggesting that the flexible bond pattern at the interface facilitates the incorporation of this defect complex.

In correspondence of the calculated defect level, the experimental density of interface states shows a small peak to which an acceptor character has been associated [6]. This measurement has been done using a *n*-type capacitor and is thus not sensitive to a possible donorlike behavior of the defect. The $(As_{Ga})_2$-$O_{As}$ defect can thus not be ruled out as possible origin of the defect states lying close to conduction band minimum.

### C. $V_{Ga}$-$As_{Ga}$/$V_{As}$-2 $As_{Ga}$ defect complex

The $V_{Ga}$-$As_{Ga}$/$V_{As}$-2 $As_{Ga}$ defect complex has two different stable forms [49]. The $V_{Ga}$-$As_{Ga}$ form results from the binding of a $V_{Ga}$ and a $As_{Ga}$. This form of the defect can then transform to the $V_{As}$-2 $As_{Ga}$ form via the displacement of one As atom neighboring the gallium vacancy into $V_{Ga}$:

$$V_{Ga}\text{-}As_{Ga} \rightleftharpoons 2\,As_{Ga}\text{-}V_{As}. \tag{6}$$

In the bulk, this defect is amphoteric and bistable as the structure on the left-hand side is stable in negative charge states and spontaneously transforms into the structure on the right-hand side in positive charge states [49]. This defect complex has been invoked in order to explain the Fermi-level pinning observed in highly irradiated GaAs [49].

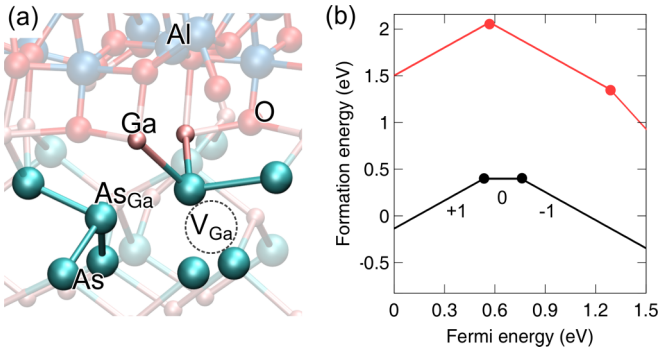


FIG. 6. (Color online) (a) Relaxed structure of the distorted $V_{Ga}$-$As_{Ga}$ defect in the charge state −1. (b) Formation energy of the $V_{Ga}$-$As_{Ga}$/$V_{As}$-2 $As_{Ga}$ defect complex vs Fermi energy as obtained through the use of model I of the GaAs/$Al_2O_3$ interface (black lines) and of a bulk model (red lines). As-rich conditions are assumed.

We here study the $V_{As}$-2 $As_{Ga}$ defect complex in the proximity of the GaAs/oxide interface. This form is found to be stable in the charge state +1. Its structure closely resembles the $(As_{Ga})_2$-$O_{As}$ defect but lacks the O atom saturating the Ga DBs. The electron counting rule is satisfied by the formation of a stretched Ga-Ga bond, which captures the 1/2 electrons released by the As-As bonds formed by the two As antisites. The addition of one electron leads to a distorted form of the $V_{Ga}$-$As_{Ga}$ defect, which is then essentially maintained in the charge state −1. The presence of the interface favors a distortion by which one of the As atoms neighboring the $As_{Ga}$ forms a bond to an As atom of the network rather than to the $As_{Ga}$, as shown in Fig. 6(a) for the −1 charge state. From the electronic point of view, this atomic configuration does not differ from the bulk form of the $V_{Ga}$-$As_{Ga}$ defect, as it shows the same amount of As-As bonds and As DBs. Accordingly, the electron counting rule is satisfied in this charge state.

The formation energies vs Fermi energy for these defect complexes are shown in Fig. 6(b). Calculated finite-size correction energies amount to 0.10 eV for the singly positive and negative charge states. It is remarkable to point out that this defect complex undergoes strong stabilization in proximity of the interface, with a reduction of the formation energies between 1.66 eV (in *p*-type conditions) and 1.29 eV (in *n*-type conditions) with respect to corresponding bulk values.[3] This confers strong stability to this defect even compared to the interfacial $As_{Ga}$: in *p*-type conditions the formation energies differ by less than 0.2 eV, but the $V_{Ga}$-$As_{Ga}$ defect complex is more stable than the $As_{Ga}$ by as much as 1.43 eV in *n*-type conditions. The overall electronic behavior of the defect complex at the interface differs from that of its bulk counterpart insofar the −2 charge state is no longer found to be stable at

[3]The present results for the bulk defect obtained with a 64-atom supercell agree with those of Ref. [49] obtained with a larger supercell.

the interface. The $+1/-1$ defect level of the interface defect is found at 0.65 eV above the GaAs VBM, close to the respective value for the bulk defect at 0.55 eV. Unlike for the bulk defect, we find that the neutral charge state of the interface defect is stable in a narrow range of Fermi energies, between 0.53 and 0.76 eV above the GaAs VBM.

The dominant structural rearrangements involved in the charge capture/release process underlying the amphoteric behavior of this defect can be best rationalized by considering the $+1$ and the $-1$ defect states where the electron counting rule is perfectly satisfied. The process can be described by the combination of two net reactions. The first one corresponds to the bistability of the As dimer/DB defect and is electrically active:

$$\text{As-As} \underset{-2e^-}{\overset{+2e^-}{\rightleftharpoons}} 2\,\text{DB}^{\bullet}_{\text{As}}, \tag{7}$$

while the second reaction represents the suppression of homopolar bonds in favor of regular Ga–As bonds without any electron transfer:

$$\text{As-As} + \text{Ga-Ga} \rightleftharpoons 2\,\text{Ga-As}. \tag{8}$$

For the $V_{Ga}$-$As_{Ga}$/$V_{As}$-2 $As_{Ga}$ defect complex, the $+1/-1$ charge transition occurs at about 0.6 eV above the GaAs VBM for both the interface and bulk defect. However, the charge transition level of the $(As_{Ga})_2$-$O_{As}$ defect, which is also governed by Eq. (7), occurs at much higher energies, namely at 1.19 eV above the GaAs VBM. We explain this behavior through Eq. (8), which energetically favors the right-hand side of the reaction. This stabilizes the negative defect state with respect to the positive one, and thus results in a lower defect level.

The amphoteric nature of the defect complex drives the Fermi level towards midgap, where the neutral charge state of the interface defect is stable. The $+1/0$ and $0/-1$ defect levels fall close to the midgap peaks in the experimental $D_{it}$ [4–6]. The $+1/0$ and $0/-1$ defect levels show donorlike and acceptorlike behavior, respectively, in accord with actual observations [6]. These defect levels thus show overall consistency with the midgap peaks in the $D_{it}$.

## IV. INTERFACIAL DEFECTS

### A. Ga DB defect

A subsurface Ga dangling bond is modeled at the $GaAs/Al_2O_3$ interface through the formation of a cavity in model I of the $GaAs/Al_2O_3$ interface, as shown in Fig. 7(a). After removing an interfacial As atom and a subsurface Ga atom, we saturate the undesired DBs with H atoms making sure that the electron counting rule is satisfied, in a similar way as described in Ref. [42]. Indeed, the three created H-As bonds release 3/4 electrons, while the two Ga-H bonds capture 2/4 electrons. The remaining 1/4 electrons are captured by the Ga DB, which then becomes singly occupied in the neutral supercell ($Q = 0$). In this defect configuration, the defect charge is $q = -1/4$ and the secondary structural units carry a charge of $q' = 1/4$. We also consider the unoccupied dangling bond, with a defect charge of $q = +0.75$ and a supercell charge of $Q = +1$.

Upon charging the dangling bond, the defect charge changes sign going from $q = +0.75$ in the unoccupied state to $q = -0.25$ in the singly occupied state. This clearly reveals the amphoteric nature of the Ga DB defect. In the singly occupied state, the average Ga-As bond length formed by the Ga atom carrying the dangling bond is 2.48 Å, very close to the bulk Ga-As bond length of 2.45 Å [cf. Fig. 7(a)]. In the unoccupied DB state, this average bond length reduces to 2.37 Å upon structural relaxation.

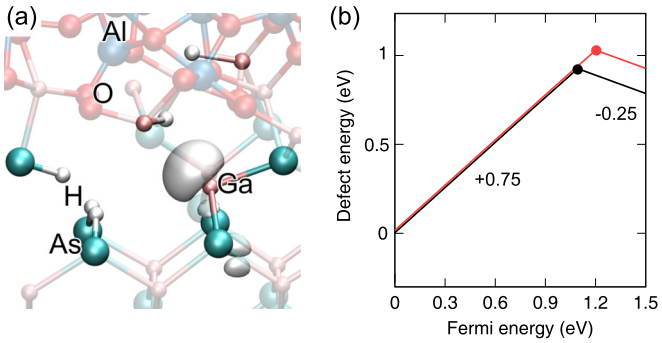


FIG. 7. (Color online) (a) Relaxed structure of the Ga DB defect at the $GaAs/Al_2O_3$ interface. The charge density of the singly occupied defect state is shown in transparency. (b) Defect energy of the Ga DB defect as obtained through the use of model I of the $GaAs/Al_2O_3$ interface (black lines) and of a bulk model (from Ref. [36], red lines).

The defect energies vs Fermi energy are given in Fig. 7(b). For the supercell in the charge state $Q = +1$, we find the finite-size correction to be negligible (0.01 eV). The calculated defect level $\varepsilon_{0.75/-0.25}$ lies at 1.09 eV above the bulk GaAs VBM. The present result is close to previous calculations performed for a DB in bulk GaAs [36] [cf. Fig. 7(b)] or in an As-terminated GaAs/oxide interface model [42]. All these results agree in locating the defect level of the Ga DB defect in the upper part of the GaAs band gap. In this energy region, the experimental density of interface states only shows a small peak [4,6]. Therefore, the Ga DB defect could be at the origin of this experimental feature.

### B. As DB defect

An As dangling bond is modeled at the $GaAs/Al_2O_3$ interface through the creation of a cavity in model I of the $GaAs/Al_2O_3$ interface, as shown in Fig. 8(a). After removing one interfacial Ga atom and one interfacial O atom, one H atom is inserted to saturate the undesired As dangling bond. In this model, the compensating structural units consist of the saturated As-H bond and of the interfacial rearrangements upon which a fivefold coordinated Ga atom becomes fourfold coordinated supplying half an electron. In our model, the As DB state is doubly occupied ($q = -3/4$) in the neutral supercell ($Q = 0$) and is singly occupied ($q = +1/4$) when the supercell is charged with a total charge $Q = +1$.[4] In the doubly occupied defect state shown in Fig. 8(a), the average bond length of the As-Ga bonds involving the As atom carrying the

[4]Upon structural relaxation of the singly occupied DB state, we constrain the H-As bond length to control the electron counting and to avoid more involved structural relaxations.

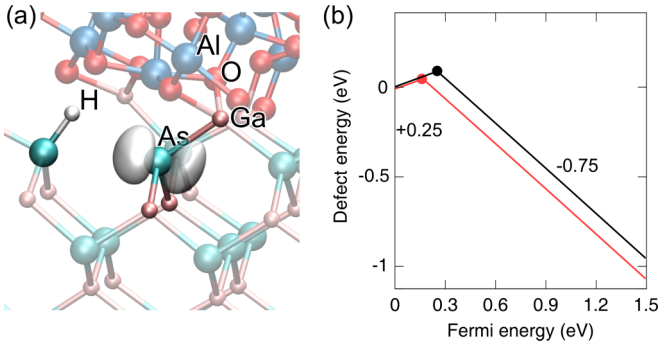


FIG. 8. (Color online) (a) Relaxed structure of the As DB defect at the $GaAs/Al_2O_3$ interface. The charge density of the doubly occupied defect state is shown in transparency. (b) Defect energy of the As DB defect as obtained through the use of model I of the $GaAs/Al_2O_3$ interface (black lines) and of a bulk model (from Ref. [36], red lines).

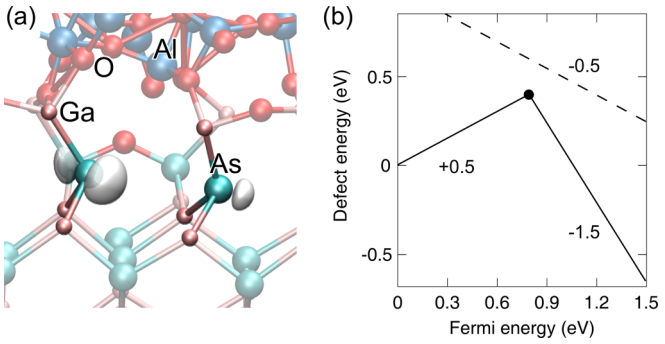


FIG. 9. (Color online) (a) Relaxed structure of the 2 $DB^{\bullet}_{As}$ defect state of the As-As dimer/DB defect. (b) Defect energy of As-As dimer/DB defect and of the metastable $(As\text{-}As)^{\star}$ defect state as obtained through the use of model II of the $GaAs/Al_2O_3$ interface.

DB is 2.40 Å and undergoes minimal variation upon removal of one electron.

The defect energies vs Fermi energy are given in Fig. 8(b). A finite-size correction of 0.16 eV is applied to the defect energy of the singly occupied DB state obtained with a total charge $Q = +1$ in the supercell. The calculated charge transition level $\varepsilon_{0.25/-0.75}$ is found at 0.25 eV above the GaAs VBM, in good agreement with a previous result obtained for an As DB in bulk GaAs [36] [cf. Fig. 8(b)]. This defect thus offers an interpretation for the origin of the small peak in the $D_{it}$ close to the VBM [4,6].

### C. As-As dimer/DB defect

An isolated As-As dimer/DB defect is modeled at the $GaAs/Al_2O_3$ interface as described in Sec. II B. The application of the electron counting rule shows that each As-O-As or As-As interfacial unit releases half an electron while each Ga-O-Ga interfacial unit captures half an electron. In the neutral supercell, our interface model contains an As-As dimer defect carrying a local charge $q = 0.5$ and compensating structural units with a global charge $q' = -0.5$ corresponding to the interfacial Ga-O-Ga and As-O-As units [40,43]. As shown previously [43], the As-As dimer undergoes bond breaking upon the capture of two electrons leading to the formation of two doubly occupied As dangling bonds ($2\,DB^{\bullet}_{As}$). The electron counting rule assigns a charge state of $q = -1.5$ to the $2\,DB^{\bullet}_{As}$ configuration. When the two extra electrons are removed, the reaction spontaneously reverts upon structural relaxation. The As-As dimer and the $2\,DB^{\bullet}_{As}$ configurations have opposite charge states and the associated defect is thus amphoteric.

In the As-As dimer defect state, the As-As bond length is 2.57 Å. The dimer can accommodate one extra electron in its antibonding state leading to a state that we denote $(As\text{-}As)^{\star}$. In this state, the As-As bond length has increased to 2.89 Å. Upon the capture of a second extra electron, the homopolar bond breaks giving rise to the $2\,DB^{\bullet}_{As}$ configuration, in which the two As atoms are separated by 4.21 Å. This charge state is illustrated in Fig. 9(a).

Figure 9(b) gives the relative defect energies of the various charge states as a function of Fermi energy.[5] Finite-size corrections applied to the $(As\text{-}As)^{\star}$ and the $2\,DB^{\bullet}_{As}$ states amount to 0.07 and 0.20 eV, respectively. The stable defect states are the As-As dimer state and the $2\,DB^{\bullet}_{As}$ state, showing a negative-$U$ behavior. The calculated charge transition level $\varepsilon_{0.5/-1.5}$ between these defect states falls at 0.79 eV above the GaAs VBM.

The $(As\text{-}As)^{\star}$ state is found to be unstable for all Fermi energies in the GaAs band gap [43]. The metastability of this defect state suggests that it does not play any role in the Fermi-level pinning, unlike previously assumed [38,40]. In the present calculation, the defect level $\varepsilon_{0.5/-0.5}$ lies at 0.99 eV above the VBM, lower by ~0.3 eV compared to the defect level found in Ref. [40] for an interface model with an As-terminated GaAs substrate.

The $\varepsilon_{0.5/-1.5}$ defect level calculated at 0.79 eV is consistent with the midgap peak at ~0.7 eV in the experimental defect density of states [4–6]. Furthermore, the amphoteric nature of the As-As dimer/DB defect naturally explains the occurrence of Fermi-level pinning through a feedback mechanism [16,43]. The description of this defect also agrees with the experimental observation that the defect states change from donorlike to acceptorlike upon the crossing of the midgap peak [6]. The dependence of the As enrichment of the surface prior to the oxide deposition [5] is a natural consequence of the As-related nature of this defect. Finally, the absence of Fermi-level pinning in MBE-grown samples could be related to the difficulty of forming an interfacial defect such as the As-As dimer/DB during these specific growth conditions, which favor bulklike reconstructions.

## V. CONCLUSIONS

In this work, we studied a set of defects susceptible to play a role in Fermi-level pinning at GaAs/oxide interfaces. All considered defects were generated within atomistic models representing the $GaAs/Al_2O_3$ interface and properly accounting for the local screening properties. In particular, we focused

[5]The present results are close to those in Ref. [43] from which they differ by the use of a denser **k**-point mesh.

on the As antisite, the $V_{Ga}$-$As_{Ga}$/$V_{As}$-2 $As_{Ga}$ complex, the $(As_{Ga})_2$-$O_{As}$ defect, the As dangling bond, the Ga dangling bond, and the As-As dimer/DB defect. These defects can be distinguished in two types. The first three defects are bulklike defects, which could either exist in the bulk or in the vicinity of the interface. For this type of defects, a pristine reference has been defined and formation energies have explicitly been evaluated. In particular, it has been possible to compare the formation energy of these defects with those of their bulk counterparts. The last three defects are interfacial defects occurring at the termination of crystalline GaAs and do not admit any bulk correspondent. For these defects, the absence of a pristine reference prevents the calculation of absolute formation energies. Nevertheless, relative defect energies associated to their various charge states and charge transition levels could still be determined.

Among the bulklike defects considered, the $(As_{Ga})_2$-$O_{As}$ defect shows the lowest formation energy. The $V_{Ga}$-$As_{Ga}$/$V_{As}$-2 $As_{Ga}$ defect complex shows low formation energies for all values of the Fermi energy, and is ∼1.4 eV more stable than the $As_{Ga}$ defect in *n*-type conditions. Since the As antisite has experimentally been observed at the interface [30], the present results suggest that the $(As_{Ga})_2$-$O_{As}$ and $V_{Ga}$-$As_{Ga}$/$V_{As}$-2 $As_{Ga}$ defects should occur at similar if not higher concentrations. Table I summarizes the formation energies of the bulklike defects considered in this work as calculated in bulk GaAs and at the GaAs/$Al_2O_3$ interface. The comparison shows that the interface systematically stabilizes the bulklike defects. The stabilization energy can be sizable involving several eV as for example in the case of the $(As_{Ga})_2$-$O_{As}$ defect, or limited to only a few tenths of eV as in the case of the As antisite.

In Table II, we summarize the charge transition levels as obtained in bulk GaAs and at the GaAs/$Al_2O_3$ interface for all the defects considered in the present work. The comparison shows that charge transition levels of defects located in the bulk or in the vicinity of the interface are generally rather close differing by at most 0.14 eV. The larger differences seen in the charge transition levels of the $V_{Ga}$-$As_{Ga}$/$V_{As}$-2 $As_{Ga}$ defect should be assigned to the structural modifications undergone by this defect at the interface.

TABLE I. Formation energies of the bulklike defects considered in the present work in their charge state $q$, as calculated in bulk GaAs and at the GaAs/$Al_2O_3$ interface. The Fermi level is taken at the VBM (*p*-type condition). The formation energies are given in eV.

| Defect | $q$ | Bulk | Interface |
|---|---|---|---|
| $As_{Ga}$ | +2 | −0.34 | −0.64 |
| | +1 | 0.18 | 0.03 |
| | 0 | 1.14 | 1.08 |
| $As^{\star}_{Ga}$ | 0 | 1.38 | 1.10 |
| $(As_{Ga})_2$-$O_{As}$ | +1 | −1.55 | −3.85 |
| | 0 | −0.29 | −2.58 |
| | −1 | 0.73 | −1.47 |
| $V_{Ga}$-$As_{Ga}$/$V_{As}$-2 $As_{Ga}$ | +1 | 1.51 | −0.15 |
| | 0 | – | 0.38 |
| | −1 | 2.65 | 1.15 |
| | −2 | 3.94 | – |

TABLE II. Charge transition levels $\varepsilon_{q1/q2}$ between the charge states $q1$ and $q2$ of the defects considered in the present work as calculated in bulk GaAs and at the GaAs/$Al_2O_3$ interface. The charge transition levels of the Ga and As DB modelled in bulk GaAs are taken from Ref. [36]. The charge transition levels are given in eV and are referenced with respect to the VBM.

| | $\varepsilon_{q1/q2}$ | Bulk | Interface |
|---|---|---|---|
| Bulklike defects | | | |
| $As_{Ga}$ | $\varepsilon_{+2/+1}$ | 0.53 | 0.67 |
| | $\varepsilon_{+1/0}$ | 0.96 | 1.04 |
| $(As_{Ga})_2$-$O_{As}$ | $\varepsilon_{+1/-1}$ | 1.14 | 1.19 |
| $V_{Ga}$-$As_{Ga}$/$V_{As}$-2 $As_{Ga}$ | $\varepsilon_{+1/0}$ | – | 0.53 |
| | $\varepsilon_{0/-1}$ | – | 0.76 |
| | $\varepsilon_{+1/-1}$ | 0.57 | – |
| | $\varepsilon_{-1/-2}$ | 1.29 | – |
| Interfacial defects | | | |
| Ga DB | $\varepsilon_{+0.75/-0.25}$ | 1.20 | 1.09 |
| As DB | $\varepsilon_{+0.25/-0.75}$ | 0.16 | 0.25 |
| As-As dimer/DB | $\varepsilon_{+0.5/-1.5}$ | – | 0.79 |

The charge transition levels of the defects are informative as they can directly be compared with the experimental $D_{it}$. In Fig. 10, the charge transition levels of the defects studied in this work are compared with various experimental measurements. The small peaks in the vicinity of the valence and conduction band edges can be associated to As and Ga dangling bonds, respectively, in accord with previous findings [36,42]. Our results reveal that the $(As_{Ga})_2$-$O_{As}$ defect also gives a defect level in the proximity of the GaAs CBM. Regarding the midgap peak, the $As_{Ga}$, the $V_{Ga}$-$As_{Ga}$/$V_{As}$-2 $As_{Ga}$ complex, and the As-As dimer/DB defect all show defect levels in the concerned energy region. Among these defects, the $As_{Ga}$ defect being a double donor is unable to account for the experimental characterization, which rather points to a defect with amphoteric character [6]. Both the $V_{Ga}$-$As_{Ga}$/$V_{As}$-2 $As_{Ga}$

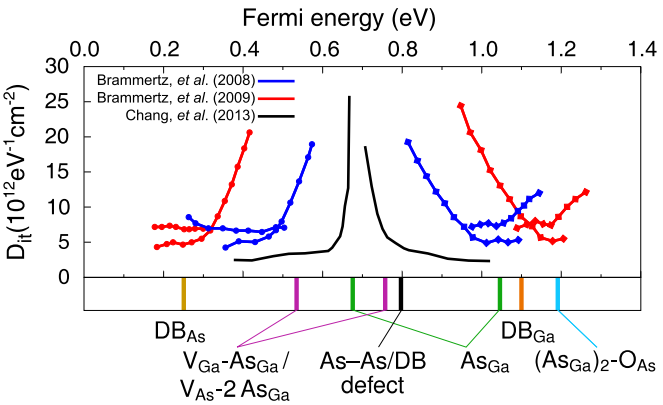


FIG. 10. (Color online) Charge transition levels of the defects considered in this study positioned with respect to the experimental $D_{it}$ at GaAs/oxide interfaces obtained by Brammertz *et al.* [4,6] (red and blue lines) and by Chang *et al.* [5] (black lines). The lines with dots indicate donor-like defects while the lines with squares indicate acceptorlike defects.

defect complex and the As-As dimer/DB defect present the observed amphoteric behavior in this region of the GaAs band gap. Interestingly, despite their very different atomic structures, both these defects exhibit the same atomistic mechanism at the origin of their amphoteric nature, namely the transformation of one As-As bond into $2\,DB^{\bullet}_{As}$ and vice versa upon the capture and release of two electrons.

To conclude, we remark that the As-As dimer/DB bistability has been found to be operative in a number of As-related defects leading to defect levels in the band gap of GaAs. The associated amphoteric behavior provides a feedback mechanism by which the Fermi level can be pinned at the charge transition level where the positively and negatively charged defect states coexist. In particular, the $V_{Ga}$-$As_{Ga}$/$V_{As}$-2 $As_{Ga}$ complex and the As-As dimer/DB defects yield defect levels at midgap and are valid candidate defects for the origin of the Fermi-level pinning at the GaAs/oxide interfaces.

## ACKNOWLEDGMENTS

Financial support is acknowledged from the Swiss National Science Foundation (Grant No. 200020-152799). We used computational resources of CSCS and CSEA-EPFL.

[1] J. A. del Alamo, Nature (London) **479**, 317 (2011).
[2] J. Nah, H. Fang, C. Wang, K. Takei, M. H. Lee, E. Plis, S. Krishna, and A. Javey, Nano Lett. **12**, 3592 (2012).
[3] M. Hong, J. Kwo, A. R. Kortan, J. P. Mannaerts, and A. M. Sergent, Science **283**, 1897 (1999).
[4] G. Brammertz, H.-C. Lin, K. Martens, D. Mercier, S. Sioncke, A. Delabie, W. E. Wang, M. Caymax, M. Meuris, and M. Heyns, Appl. Phys. Lett. **93**, 183504 (2008).
[5] Y. C. Chang, W. H. Chang, C. Merckling, J. Kwo, and M. Hong, Appl. Phys. Lett. **102**, 093506 (2013).
[6] G. Brammertz, H. C. Lin, K. Martens, A.-R. Alian, C. Merckling, J. Penaud, D. Kohen, W.-E. Wang, S. Sioncke, A. Delabie, M. Meuris, M. R. Caymax, and M. Heyns, ECS Trans. **19**, 375 (2009).
[7] W. E. Spicer, J. Vac. Sci. Technol. **16**, 1422 (1979).
[8] W. Spicer, P. Chye, C. Garner, I. Lindau, and P. Pianetta, Surf. Sci. **86**, 763 (1979).
[9] W. E. Spicer, I. Lindau, P. Skeath, C. Y. Su, and P. Chye, Phys. Rev. Lett. **44**, 420 (1980).
[10] W. E. Spicer, Z. Liliental-Weber, E. Weber, N. Newman, T. Kendelewicz, R. Cao, C. McCants, P. Mahowald, K. Miyano, and I. Lindau, J. Vac. Sci. Technol. B **6**, 1245 (1988).
[11] H. C. Alt, Phys. Rev. Lett. **65**, 3421 (1990).
[12] H. C. Alt, Y. V. Gomeniuk, and U. Kretzer, J. Appl. Phys. **101**, 073516 (2007).
[13] H. C. Alt, Appl. Phys. Lett. **55**, 2736 (1989).
[14] H. C. Alt, Appl. Phys. Lett. **54**, 1445 (1989).
[15] M. Jordan, M. Linde, T. Hangleiter, and J. Spaeth, Semicond. Sci. Technol. **7**, 731 (1992).
[16] W. Walukiewicz, J. Vac. Sci. Technol. B **5**, 1062 (1987).
[17] W. Walukiewicz, Physica B **302-303**, 123 (2001).
[18] W. Walukiewicz, Phys. Rev. B **37**, 4760 (1988).
[19] C. L. Hinkle, A. M. Sonnet, E. M. Vogel, S. McDonnell, G. J. Hughes, M. Milojevic, B. Lee, F. S. Aguirre-Tostado, K. J. Choi, J. Kim, and R. M. Wallace, Appl. Phys. Lett. **91**, 163512 (2007).
[20] J. P. d. Souza, E. Kiewra, Y. Sun, A. Callegari, D. K. Sadana, G. Shahidi, D. J. Webb, J. Fompeyrine, R. Germann, C. Rossel, and C. Marchiori, Appl. Phys. Lett. **92**, 153508 (2008).
[21] C. L. Hinkle, A. M. Sonnet, E. M. Vogel, S. McDonnell, G. J. Hughes, M. Milojevic, B. Lee, F. S. Aguirre-Tostado, K. J. Choi, H. C. Kim, J. Kim, and R. M. Wallace, Appl. Phys. Lett. **92**, 071901 (2008).
[22] C. L. Hinkle, M. Milojevic, B. Brennan, A. M. Sonnet, F. S. Aguirre-Tostado, G. J. Hughes, E. M. Vogel, and R. M. Wallace, Appl. Phys. Lett. **94**, 162101 (2009).
[23] M. Caymax, G. Brammertz, A. Delabie, S. Sioncke, D. Lin, M. Scarrozza, G. Pourtois, W.-E. Wang, M. Meuris, and M. Heyns, Microelectron. Eng. **86**, 1529 (2009).
[24] R. M. Wallace, P. C. McIntyre, J. Kim, and Y. Nishi, MRS Bull. **34**, 493 (2009).
[25] E. O'Connor, S. Monaghan, R. D. Long, A. O'Mahony, I. M. Povey, K. Cherkaoui, M. E. Pemble, G. Brammertz, M. Heyns, S. B. Newcomb, V. V. Afanas'ev, and P. K. Hurley, Appl. Phys. Lett. **94**, 102902 (2009).
[26] Y. C. Chang, C. Merckling, J. Penaud, C. Y. Lu, W.-E. Wang, J. Dekoster, M. Meuris, M. Caymax, M. Heyns, J. Kwo, and M. Hong, Appl. Phys. Lett. **97**, 112901 (2010).
[27] C. Hinkle, E. Vogel, P. Ye, and R. Wallace, Curr. Opin. Solid St. M. **15**, 188 (2011).
[28] W. Cabrera, B. Brennan, H. Dong, T. P. O'Regan, I. M. Povey, S. Monaghan, E. O'Connor, P. K. Hurley, R. M. Wallace, and Y. J. Chabal, Appl. Phys. Lett. **104**, 011601 (2014).
[29] W. Wang, C. Gong, B. Shan, R. M. Wallace, and K. Cho, Appl. Phys. Lett. **98**, 232113 (2011).
[30] A. Stesmans, S. Nguyen, and V. V. Afanas'ev, Appl. Phys. Lett. **103**, 162111 (2013).
[31] M. Passlack, M. Hong, and J. P. Mannaerts, Appl. Phys. Lett. **68**, 1099 (1996).
[32] M. Hong, M. Passlack, J. P. Mannaerts, J. Kwo, S. N. G. Chu, N. Moriya, S. Y. Hou, and V. J. Fratello, J. Vac. Sci. Technol. B **14**, 2297 (1996).
[33] M. Passlack, M. Hong, J. Mannaerts, R. Opila, S. Chu, N. Moriya, F. Ren, and J. Kwo, IEEE Electron Dev. **44**, 214 (1997).
[34] D. L. Winn, M. J. Hale, T. J. Grassman, J. Z. Sexton, A. C. Kummel, M. Passlack, and R. Droopad, J Chem. Phys. **127**, 134705 (2007).
[35] J. Robertson, Appl. Phys. Lett. **94**, 152104 (2009).
[36] H.-P. Komsa and A. Pasquarello, Appl. Phys. Lett. **97**, 191901 (2010).
[37] W. Wang, K. Xiong, R. M. Wallace, and K. Cho, J. Appl. Phys. **110**, 103714 (2011).
[38] L. Lin and J. Robertson, Appl. Phys. Lett. **98**, 082903 (2011).
[39] J. Robertson and L. Lin, Appl. Phys. Lett. **99**, 222906 (2011).
[40] G. Miceli and A. Pasquarello, Appl. Phys. Lett. **103**, 041602 (2013).

[41] Y. Guo, L. Lin, and J. Robertson, Appl. Phys. Lett. **102**, 091606 (2013).
[42] G. Miceli and A. Pasquarello, Appl. Surf. Sci. **291**, 16 (2014).
[43] D. Colleoni, G. Miceli, and A. Pasquarello, J. Phys.: Condens. Matter **26**, 492202 (2014).
[44] J. Robertson, Y. Guo, and L. Lin, J. Appl. Phys. **117**, 112806 (2015).
[45] D. Colleoni and A. Pasquarello, Appl. Phys. Lett. **107**, 031605 (2015).
[46] H.-P. Komsa and A. Pasquarello, Microelectron. Eng. **88**, 1436 (2011).
[47] G. Miceli and A. Pasquarello, Appl. Phys. Lett. **102**, 201607 (2013).
[48] G. A. Baraff and M. Schlüter, Phys. Rev. Lett. **55**, 1327 (1985).
[49] D. Colleoni and A. Pasquarello, Microelectron. Eng. **109**, 50 (2013).
[50] J. Schneider, B. Dischler, H. Seelewind, P. M. Mooney, J. Lagowski, M. Matsui, D. R. Beard, and R. C. Newman, Appl. Phys. Lett. **54**, 1442 (1989).
[51] F. K. Koschnick, M. Linde, M. V. B. Pinheiro, and J.-M. Spaeth, Phys. Rev. B **56**, 10221 (1997).
[52] M. Linde, J.-M. Spaeth, and H. C. Alt, Appl. Phys. Lett. **67**, 662 (1995).
[53] M. Skowronski, S. T. Neild, and R. E. Kremer, Appl. Phys. Lett. **57**, 902 (1990).
[54] M. Pesola, J. von Boehm, V. Sammalkorpi, T. Mattila, and R. M. Nieminen, Phys. Rev. B **60**, R16267 (1999).
[55] D. Colleoni and A. Pasquarello, Appl. Phys. Lett. **103**, 142108 (2013).
[56] H.-P. Komsa and A. Pasquarello, Phys. Rev. B **84**, 075207 (2011).
[57] J. P. Perdew, K. Burke, and M. Ernzerhof, Phys. Rev. Lett. **77**, 3865 (1996).
[58] P. Giannozzi, S. Baroni, N. Bonini, M. Calandra, R. Car, C. Cavazzoni, D. Ceresoli, G. L. Chiarotti, M. Cococcioni, I. Dabo, A. Dal Corso, S. de Gironcoli, S. Fabris, G. Fratesi, R. Gebauer, U. Gerstmann, C. Gougoussis, A. Kokalj, M. Lazzeri, L. Martin-Samos, N. Marzari, F. Mauri, R. Mazzarello, S. Paolini, A. Pasquarello, L. Paulatto, C. Sbraccia, S. Scandolo, G. Sclauzero, A. P. Seitsonen, A. Smogunov, P. Umari, and R. M. Wentzcovitch, J. Phys: Condens. Matter **21**, 395502 (2009).
[59] H.-P. Komsa and A. Pasquarello, J. Phys.: Condens. Matter **24**, 045801 (2012).
[60] J. Heyd, G. E. Scuseria, and M. Ernzerhof, J. Chem. Phys. **118**, 8207 (2003).
[61] J. Heyd, G. E. Scuseria, and M. Ernzerhof, J. Chem. Phys. **124**, 219906 (2006).
[62] H.-P. Komsa, P. Broqvist, and A. Pasquarello, Phys. Rev. B **81**, 205118 (2010).
[63] P. Broqvist, A. Alkauskas, and A. Pasquarello, Phys. Rev. B **80**, 085114 (2009).
[64] I. Vurgaftman, J. R. Meyer, and L. R. Ram-Mohan, J. Appl. Phys. **89**, 5815 (2001).
[65] P. Dahinden, P. Broqvist, and A. Pasquarello, Phys. Rev. B **81**, 085331 (2010).
[66] G. Miceli and A. Pasquarello, Microelectron. Eng. **109**, 60 (2013).
[67] D. Colleoni, G. Miceli, and A. Pasquarello, Microelectron. Eng. **147**, 260 (2015).
[68] A. Alkauskas, P. Broqvist, and A. Pasquarello, Phys. Rev. Lett. **101**, 046405 (2008).
[69] A. Alkauskas, P. Broqvist, and A. Pasquarello, Phys. Status Solidi B **248**, 775 (2011).
[70] G. Pacchioni, F. Frigoli, D. Ricci, and J. A. Weil, Phys. Rev. B **63**, 054102 (2000).
[71] J. Lægsgaard and K. Stokbro, Phys. Rev. Lett. **86**, 2834 (2001).
[72] A. Carvalho, A. Alkauskas, A. Pasquarello, A. K. Tagantsev, and N. Setter, Phys. Rev. B **80**, 195205 (2009).
[73] J. L. Lyons, A. Janotti, and C. G. Van de Walle, Phys. Rev. Lett. **108**, 156403 (2012).
[74] M. M. Frank, G. D. Wilk, D. Starodub, T. Gustafsson, E. Garfunkel, Y. J. Chabal, J. Grazul, and D. A. Muller, Appl. Phys. Lett. **86**, 152904 (2005).
[75] D. Colleoni and A. Pasquarello, Appl. Surf. Sci. **291**, 6 (2014).
[76] C. G. Van de Walle and J. Neugebauer, J. Appl. Phys. **95**, 3851 (2004).
[77] H.-P. Komsa, T. T. Rantala, and A. Pasquarello, Phys. Rev. B **86**, 045112 (2012).
[78] C. Freysoldt, J. Neugebauer, and C. G. Van de Walle, Phys. Rev. Lett. **102**, 016402 (2009).
[79] H.-P. Komsa and A. Pasquarello, Phys. Rev. Lett. **110**, 095505 (2013).
[80] S. Adachi, J. Appl. Phys. **58**, R1 (1985).
[81] A. K. Harman, S. Ninomiya, and S. Adachi, J. Appl. Phys. **76**, 8032 (1994).
[82] K. Shiraishi, J. Phys. Soc. Jpn. **59**, 3455 (1990).
[83] J. Dabrowski and M. Scheffler, Phys. Rev. Lett. **60**, 2183 (1988).
[84] D. J. Chadi and K. J. Chang, Phys. Rev. Lett. **60**, 2187 (1988).
[85] H. D. Lee, T. Feng, L. Yu, D. Mastrogiovanni, A. Wan, T. Gustafsson, and E. Garfunkel, Appl. Phys. Lett. **94**, 222108 (2009).
[86] W. Wang, C. Hinkle, E. Vogel, K. Cho, and R. Wallace, Microelectron. Eng. **88**, 1061 (2011).
[87] T. R. Paudel, A. Zakutayev, S. Lany, M. d'Avezac, and A. Zunger, Adv. Func. Mater. **21**, 4493 (2011).